Prabhakar Venkateswaran
Department of Mechanical Engineering,
Iowa State University,
Ames, IA 50011
e-mail: pv1@iastate.edu

Andrew D. Marshall
School of Mechanical Engineering,
Georgia Institute of Technology,
Atlanta, GA 30332
e-mail: andrew.marshall@gatech.edu

Jerry M. Seitzman
School of Aerospace Engineering,
Georgia Institute of Technology,
Atlanta, GA 30332
e-mail: jerry.seitzman@ae.gatech.edu

Tim C. Lieuwen
School of Aerospace Engineering,
Georgia Institute of Technology,
Atlanta, GA 30332
e-mail: tim.lieuwen@aerospace.gatech.edu

Turbulent Consumption Speeds of High Hydrogen Content Fuels From 1–20 atm

This work describes measurements and analysis of the turbulent consumption speeds, $S_{T,GC}$, of H_2/CO fuel blends. We report measurements of $S_{T,GC}$ at pressures and normalized turbulence intensities, $u'_{rms}/S_{L,0}$, up to 20 atm and 1800, respectively, for a variety of H_2/CO mixtures and equivalence ratios. In addition, we present correlations of these data using laminar burning velocities of highly stretched flames, $S_{L,max}$, derived from quasi-steady leading points models. These analyses show that $S_{L,max}$ can be used to correlate data over a broad range of fuel compositions but do not capture the pressure sensitivity of $S_{T,GC}$. We suggest that these pressure effects are more fundamentally a manifestation of non-quasi-steady behavior in the mass burning rate at the flame leading points. [DOI: 10.1115/1.4025210]

Introduction

The turbulent flame speed, S_T, has important impacts on combustor design and behavior, including the distribution of the flame in a combustor and key operational characteristics, such as blow-off, flashback, and combustion instability [1]. S_T data can also be used to develop closure models for the mean reaction rates in Reynolds-averaged Navier–Stokes (RANS) and large eddy simulation (LES) approaches to modeling turbulent premixed combustion [2,3]. In addition, one metric for assessing combustion codes is their ability to predict S_T accurately [2,4].

This paper is a continuation of recent work by the authors to measure and model turbulent consumption speeds, $S_{T,GC}$, of hydrogen/carbon monoxide (H_2/CO) mixtures, which simulate synthesis gas (syngas) mixtures [5,6]. There are several motivators for the study of these fuels. First, there is interest in utilizing gaseous fuels derived from coal or biomass feedstocks. For example, precombustion carbon capture schemes typically involve burning a high hydrogen content fuel [7]. However, the specific composition depends upon the fuel source and processing technique, leading to substantial variability in composition—one of the largest barriers towards their usage in lean, premixed combustion systems [1]. A second motivator for the study is the widespread usage of rich-quench-lean, or RQL, combustors [8]. In these systems, the fuel-rich front end of the combustor, usually burning a liquid fuel, is followed by a lean zone burning the remaining fuel, which consists of H_2/CO and vitiated combustion products. A third motivator for this work is to more fundamentally understand preferential diffusion effects on the turbulent flame speed. This effect is particularly pronounced in high H_2 content fuels, because of the significant differences in molecular weight of H_2 relative to air.

The influence of fuel composition on S_T has been widely reported in the literature and is the subject of a focused review [9]. For example, in the work by Kido et al. [10], various mixtures of H_2, methane (CH_4), and propane (C_3H_8) with the same unstretched laminar flame speed, $S_{L,0}$, were shown to have substantially different S_T values. We reported similar findings with various H_2/CO mixtures at pressures up to 5 atm and normalized turbulence intensities, $u'_{\rm rms}/S_{L,0}$, up to 45 [5,6]. Thus, classical correlations of the form $S_T = S_T\left(u'_{\rm rms}, S_{L,0}\right)$ [2] are inadequate across a range of fuel blends with significantly different molecular weights.

The observed fuel sensitivities of S_T have been attributed to the reactant mixture stretch sensitivity. For example, high H_2 content fuels are very stretch sensitive, due to the high mass diffusivity of H_2. This leads to variations in the local burning velocity along the turbulent flame front due to nonunity Lewis number and preferential diffusion effects [11]. To incorporate this effect, some workers have included stretch sensitivity characteristics into correlations by using the mixture Markstein length, l_M, defined by Eq. (1) and indicated in Fig. 2 [12–14].

$$l_M = \left.\frac{\partial S_L}{\partial \kappa}\right|_{\kappa=0} \tag{1}$$

These approaches capture some aspects of the fuel composition sensitivity of S_T, as measurements typically show increased turbulent flame speeds with increasing stretch sensitivity [4,10,14]. However, a Markstein length scaling does not capture coupled fuel composition and pressure effects, as increasing pressure decreases Markstein lengths by thinning the flame, as seen in Fig. 2. Different measurements show that pressure both increases and has no effect on turbulent burning velocities [15,16]; a Markstein length scaling argument would predict that increasing pressure, and thereby decreasing Markstein lengths, should decrease turbulent burning velocities.

Other analyses have argued for the dynamical significance of a different measure of the stretch sensitivity of the flame—the maximum laminar burning velocity over all stretch rates, $S_{L,\max}$, also indicated in Fig. 2 [9,17]. This is also a measure of the mixture's stretch sensitivity but focuses on the high stretch characteristics

Contributed by the Combustion and Fuels Committee of ASME for publication in the Journal of Engineering for Gas Turbines and Power. Manuscript received July 20, 2013; final manuscript received July 27, 2013; published online October 21, 2013. Editor: David Wisler.

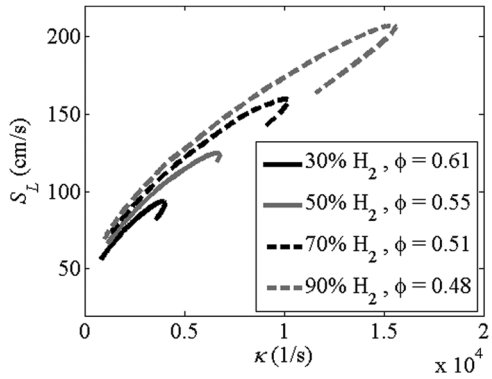

Fig. 1 Mixture stretch sensitivity for different H_2/CO mixtures of constant $S_{L,0}$ at 1 atm

(as $S_{L,\max}$ occurs at flame stretch rates, κ, close to extinction, κ_{ext}), rather than its low stretch sensitivity, as captured by the Markstein length. Depending upon the quantity being varied, the Markstein length and $S_{L,\max}$ can have similar or quite different characteristics. For example, both increase with increasing H_2 content of the fuel, as shown in Fig. 1. However, l_M decreases with pressure, while $S_{L,\max}$ stays nearly constant, as shown in Fig. 2.

The suggestion that S_T is controlled by $S_{L,\max}$ was derived from leading points arguments [9,18,19]. Leading points, which are loosely defined as positively curved points on the turbulent flame front that propagate out furthest into the reactants, are a natural framework to incorporate stretch effects into turbulent combustion modeling [9,18–20]. Leading points have origins in the Kolmogorov–Petrovski–Piskunov (KPP) theory, which relates the turbulent flame speed of a statistically 1D flame residing in a prescribed statistically stationary turbulent flow field to the average reaction rate at the leading edge of the flame brush [3,21]. As a result, some authors have hypothesized that the dynamics of these points control the overall propagation velocity of the turbulent flame [9], a result that can also be derived for isodensity fronts in slowly evolving turbulent flow fields [5]. For negative Markstein length mixtures, the burning rate of this positively curved leading point increases [11]. If the turbulent burning velocity is indeed controlled by the leading point characteristics [18], the ensemble-averaged laminar burning rate of this leading point is a very significant turbulent flame property.

Using leading points concepts, we previously developed an inequality for the turbulent flame speed [5] that is similar to the classical Damköhler turbulent flame speed scaling [22], except the

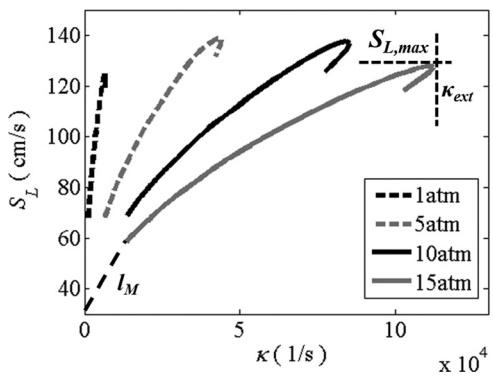

Fig. 2 Pressure effect on mixture stretch sensitivity for 50% H_2 mixtures at constant $S_{L,0}$

parameter arising from the analysis is the maximum stretched laminar flame speed, $S_{L,\max}$ [5],

$$\frac{S_T}{S_{L,\max}} \leq 1 + \frac{\langle u'_{\rm rms}\rangle_{\rm LP}}{S_{L,\max}} \tag{2}$$

This inequality can be replaced by an equality in certain situations. If the mixtures are thermodiffusively unstable, $S_{L,0}$ is a "repelling" point, since a positively curved perturbation on a flat flame will grow with increasing curvature and correspondingly increasing flame speeds. In fact, it can be rigorously shown that $S_{L,\max}$ is a steady-state "attracting" point for constant density flames with positively curved wrinkles [5]. As such, if the turbulent eddies evolve over a time scale that is slow relative to that required for the leading points to be attracted to the $S_{L,\max}$ point, then Eq. (2) can be replaced by an equality.

When applied to our data, Eq. (2) was able to collapse the data across all H_2/CO and equivalence ratio values at a given pressure. However, it was not able to collapse data taken at different pressures (1, 5, and 10 atm) [6]. To interpret this result, we pointed out that $S_{L,\max}$ is not an intrinsic property of the reactant mixture. For example, the burning velocity of highly stretched flames is a function of the manner in which the flame is stretched (i.e., by tangential flow straining or curvature), as well as the stretch profile through the flame (manifested by, for example, moderate sensitivities of $S_{L,\max}$ or κ_{ext} to the opposed flow nozzle separation distance or velocity profile) [23]. To address this sensitivity, we performed expanding cylindrical flame and tubular flame computations, which indicate that $S_{L,\max}$ varies by about 20%–40%, depending upon the manner in which the flame stretch is applied [24].

In addition, very different $S_{L,\max}$ values are obtained when using consumption and displacement based burning velocities [25]. Finally, $S_{L,\max}$ is itself a frequency-dependent quantity [26]; the steady state values used here are only appropriate if the internal structure of the leading point is quasi-steady. Since a factor of ten increase in the pressure results in a similar reduction in the chemical time scale, this shows that pressure effects can substantially alter the degree of non-quasi-steadiness of the internal structure of the flame leading point [6], as discussed further in the analysis portion of this paper. However, it was clear that more pressure data was required to further understand the coupled effects of fuel composition and pressure on S_T.

In this paper, we report new $S_{T,\rm GC}$ measurements at pressures of 1–20 atm and a broader fuel composition range. These $S_{T,\rm GC}$ data are significant contributions to the literature, due to limited data that explore coupled fuel and pressure effects. We next briefly summarize several of these existing data sets. Turbulent consumption speed measurements of lean CH_4/air flames for a pressure range of 1–30 atm were reported by Kobayashi et al. [16]. It was concluded that $S_{T,\rm GC}/S_{L,0}$ increased with pressure, due to $S_{L,0}$ decreasing, but that $S_{T,\rm GC}$ itself was independent of pressure. Kitagawa et al. [27] reported measurements of turbulent flame speeds of H_2/air mixtures at pressures ranging from 1–5 atm. They found that pressure had an influence on $S_T/S_{L,0}$ through the pressure effect on $S_{L,0}$. However, the influence on S_T is unclear. Daniele et al. [15] report $S_{T,\rm GC}$ measurements of H_2/CO mixtures for pressures of 1–20 atm at 623 K. They found that $S_{T,\rm GC}/S_{L,0}$ increased with pressure at each given H_2/CO ratio and $u'_{\rm rms}/S_{L,0}$ value. Furthermore, $S_{T,\rm GC}$ was seen to be practically independent of pressure for a fixed H_2/CO ratio and equivalence ratio. More recently, Liu et al. [28] reported turbulent flame speed measurements of a $\phi = 0.8$, CH_4/air mixture and Chiu et al. [29] reported turbulent flame speed measurements of a $\phi = 0.5$, H_2/CO/air mixture where H_2/CO = 35/65 at pressures up to 10 atm. Both studies conducted spherical-bomb experiments, where the turbulent Reynolds number, Re_t, was held constant across the pressures by simultaneously varying the

turbulence intensity, u'_{rms} and turbulent integral length scale, l_{int}. They reported that, for both CH_4/air and H_2/CO/air mixtures, S_T decreased with pressure at constant Re_t, while S_T increased with Re_t at a fixed pressure. Thus, it seems clear that pressure effects on turbulent flame speeds are not well understood, a key motivator for the work presented in the rest of this paper.

Experimental Approach and Facility

The turbulent flame speed is a definition-dependent quantity. It can be defined locally at a single point on the flame or globally averaged over the entire flame. In addition, the propagation rate can be defined based on a kinematic argument through the flow velocity at the flame front or a consumption rate. The International Workshop on Turbulent Premixed Flames [30] and recent reviews [4,31] have proposed four definitions of the turbulent flame speed: local consumption speed, $S_{T,LC}$; global consumption speed, $S_{T,GC}$; local displacement speed, $S_{T,LD}$; and global displacement speed, $S_{T,GD}$.

Experimental Facility. This study focuses upon measurements of $S_{T,GC}$ using a turbulent Bunsen flame, an $S_{T,GC}$ measurement approach recommended by Gouldin and Cheng [30]. The experimental facility has been detailed extensively in our previous work [5,32], so only a short description is provided here. A schematic of the system is shown in Fig. 3. The burner is a smoothly contoured nozzle with high contraction ratio to inhibit boundary layer growth and achieve a top-hat exit velocity profile. Measurements were taken using 12 and 20 mm exit diameter burners. An annular-sintered plate is placed around the burner outlet to hold a premixed, CH_4/air pilot flame to stabilize the main flame. The total mass flow rate of the pilot does not exceed 5% of the main flow rate to ensure minimal impact of the pilot on the main flame. The burner is placed inside a pressure vessel with four orthogonal quartz windows, each providing viewing areas of $7'' \times 2''$.

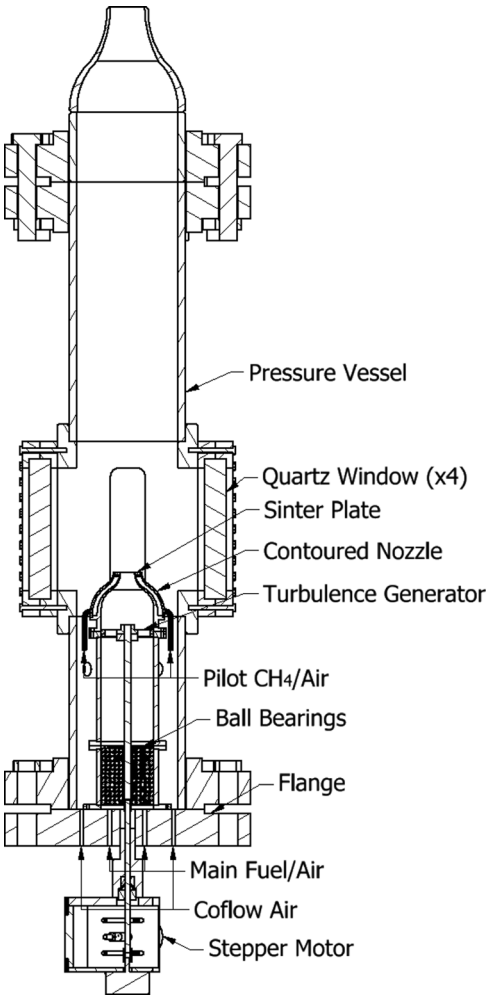

Fig. 3 Schematic of the experimental facility

The turbulence intensity is varied independently of the mean flow velocity using a remotely operable turbulence generator. Further description of the turbulence generator can be found in Marshall et al. [32].

Image Analysis. The image processing methodology is described in Ref. [5] but is briefly overviewed here. Global consumption speeds were calculated using Eq. (3), in which the key measurement input is the progress variable surface area, $\bar{A}_{\langle c \rangle}$,

$$S_{T,GC} = \frac{\dot{m}_R}{\rho_R \bar{A}_{\langle c \rangle}} \tag{3}$$

Digital images of the flame chemiluminescence were captured with a 16-bit intensified charge-coupled device camera. Line-of-sight images of the flame were obtained over 5 seconds and time-averaged. To estimate the time-averaged flame brush location from the line-of-sight images, a three-point Abel deconvolution scheme [33] was used. The axial distribution of the centerline intensity was then fit to a Gaussian curve, from which the location of the maximum intensity was identified. This point is associated with the most probable location of the flame and defined as the $\langle c \rangle = 0.5$ progress variable contour. The estimated uncertainty in identifying this point is 1%–2%. Straight lines are then drawn from this point to the two flame anchoring points and rotated about the line of symmetry to generate a cone (i.e., the "angle method" [16,34,35]). The overall uncertainty in the $S_{T,GC}$ value is estimated to be 3%.

Results

Experimental Conditions. Measurements of $S_{T,GC}$ have been obtained at pressures of 1–20 atm as a function of $u'_{rms}/S_{L,0}$ using the 12 and 20 mm diameter burner. Data were acquired at mean flow velocities of 15–50 m/s and H_2/CO ratios ranging from 30/70–90/10 by volume. Experiments were conducted where $S_{L,0}$ and reactant temperature were held fixed at 34 cm/s and 300 K, respectively. $S_{L,0}$ was kept nominally constant by adjusting the stoichiometry at each H_2/CO ratio. $S_{L,0}$ estimates were determined using the PREMIX module [36] in CHEMKIN with the Davis H_2/CO mechanism for H_2/CO mixtures [37]. A second set of experiments were also conducted, where the H_2/CO ratio, equivalence ratio, and pressure were all varied in such a way that $S_{L,0}$ was not constant across the conditions. Tables 1 and 2 summarize the experimental conditions and plotting legends for the constant $S_{L,0}$ and

Table 1 Experimental conditions and plotting legend for constant $S_{L,0}$ data set obtained using 12 and 20 mm diameter burners. Pressure data are represented by filled symbols, and the fill color is indicated by the cell color for ϕ in the leftmost column.

U_0 (m/s)	4, 10, 20, 30, 50				
H_2 (%)	30	50	70	90	CH_4
Symbol	○	◁	▷	◇	✚
ϕ, 1 atm	0.61	0.55	0.51	0.48	0.90
ϕ, 5 atm	0.75	0.68	0.63	0.59	
ϕ, 10 atm	0.84	0.75	0.70	0.66	
$S_{L,0}$ (m/s)	0.34				

Table 2 Experimental conditions and plotting legend for varying $S_{L,0}$ data set obtained using the 20 mm diameter burner. Pressure data are represented by filled symbols, and the fill color is indicated by the cell color for ϕ in the leftmost column.

U_o (m/s)	4, 10, 15, 20, 25, 30, 50			
H_2 (%)	30	50	60	70
Symbol	○	◁	□	▷
ϕ, 1 atm	0.61, 0.70, 0.80		0.40, 0.60, 0.80	
ϕ, 5 atm	0.55, 0.61	0.45, 0.50		
ϕ, 10 atm	0.57	0.40		0.40
ϕ, 20 atm		0.50		0.32, 0.40

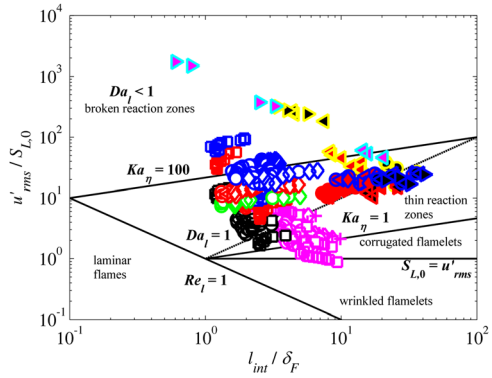

Fig. 4 Location of all the data reported in this study (12 and 20 mm) on the Borghi–Peters diagram

varying $S_{L,0}$ data. Figure 4 summarizes where the measured data are located on a Borghi–Peters diagram [38,39] for the 12- and 20-mm data. The Karlovitz number in Fig. 4 is defined as

$$Ka_\eta = \frac{\left(u'_{\text{rms}}/S_{L,0}\right)^{3/2}}{\left(l_{\text{int}}/\delta_F\right)^{1/2}} \tag{4}$$

Stretch Sensitivity Calculations. Stretch sensitivity calculations, examples of which are given in Figs. 1 and 2, were performed for the mixtures investigated in Tables 1 and 2. The stretch sensitivities were calculated using an opposed flow calculation of two premixed flames with a nozzle separation distance of 20 mm using the OPPDIF [40] module in CHEMKIN. An arc length continuation method was used to determine the extinction point. From these calculations, various stretched properties of the flame were extracted, as shown in Fig. 2. In this paper, the displacement laminar flame speed is considered, determined from the minimum velocity just upstream of the reaction zone as suggested by Wu and Law [41].

Constant $S_{L,0}$ Studies. In this section, we report $S_{T,\text{GC}}$ data acquired using the 12 mm diameter burner for pressures up to 10 atm. These data were acquired by simultaneously adjusting the H_2/CO ratio and equivalence ratio to maintain the same mixture $S_{L,0}$ of 34 cm/s [5,6]. Similar experiments were conducted with the 20 mm diameter burner as well [5], and the data have been reproduced in the Appendix for reference. Figure 5 plots $S_{T,\text{GC}}$ as a function of u'_{rms} normalized by $S_{L,0}$ for the range of conditions reported in Table 1.

A few interesting observations can be made from Fig. 5. Firstly, note that the "fuel effects" discussed in the introduction are present at all pressures. In other words, different H_2/CO blends at constant $S_{L,0}$ and u'_{rms} have different turbulent flame speeds. In our earlier work, we made similar observations but for data up to

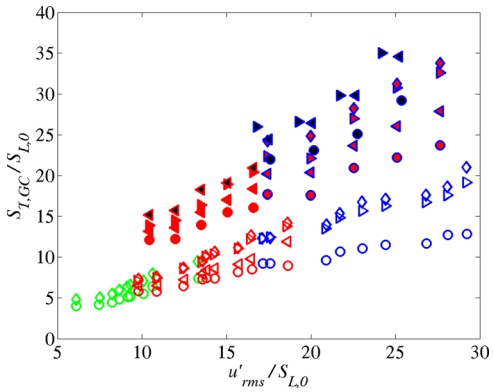

Fig. 5 $S_{T,\text{GC}}$ as a function u'_{rms} normalized by $S_{L,0}$ at various mean flow velocities, H_2/CO ratios, and pressures for the 12 mm diameter burner (see Table 1 for legend)

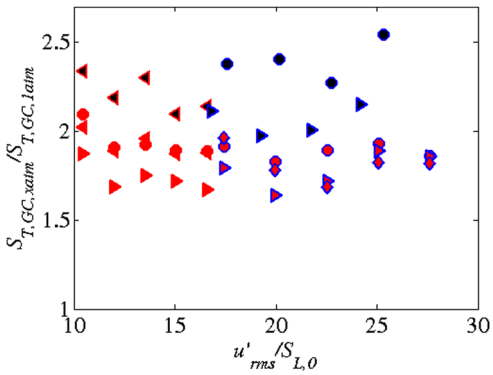

Fig. 6 Ratio of $S_{T,\text{GC}}$ at 5 and 10 atm to 1 atm across the range of turbulence intensities investigated

5 atm [6]. Second, increasing pressure leads to increased turbulent flame speed (i.e., at constant $S_{L,0}$ and u'_{rms}, $S_{T,\text{GC}}$ increases with pressure). This increase is quantified in Fig. 6, which plots the ratio of $S_{T,\text{GC}}/S_{L,0}$ at 5 and 10 atm to 1 atm for each mixture and mean flow velocity as a function of turbulence intensity. This ratio has values of about 1.8–2.1 and 2.2–2.5 at 5 and 10 atm, respectively. Note that this is not an $S_{L,0}$ effect, as $S_{L,0}$ is kept fixed at 34 cm/s.

Varying $S_{L,0}$ Studies. In this section, we report $S_{T,\text{GC}}$ data acquired using the 20 mm burner for the conditions given in Table 2. In particular, we have obtained data at pressures up to 20 atm. In these experiments, the H_2/CO ratio was held fixed, while the equivalence ratio was varied. The data obtained from this study conducted at 1 atm were previously reported in Ref. [5] but have been reproduced in Figs. 17 and 18 in the Appendix for reference. Figures 7 and 8 plot these data on a linear and log-log plot, respectively.

There are a few interesting things to note from this data. Firstly, data have been acquired at $u'_{\text{rms}}/S_{L,0}$ up to almost 2000, which is some of the highest reported normalized turbulence intensities at which S_T data have been acquired. However, this large value is due to the very low computed values of $S_{L,0}$, which at 20 atm and $\phi = 0.32$ equals 0.14 cm/s. There is some question as to the value of $S_{L,0}$ for these very lean high pressure mixtures, since in reality these flames typically display cellular structures, rendering the determination of $S_{L,0}$ impossible [11]. As a result, chemical kinetic mechanisms, such as the one used in these calculations, are not optimized for such conditions and the calculated values of $S_{L,0}$ need to be regarded with caution.

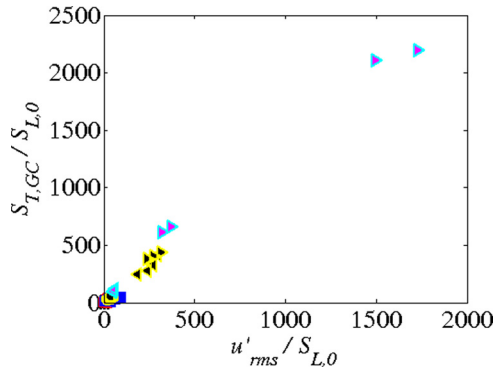

Fig. 7 Linear plot of $S_{T,GC}$ as function of u'_{rms} normalized by $S_{L,0}$ at various mean flow velocities, H_2/CO ratios, and pressures for the 20 mm diameter burner (see Tables 1 and 2 for the legend)

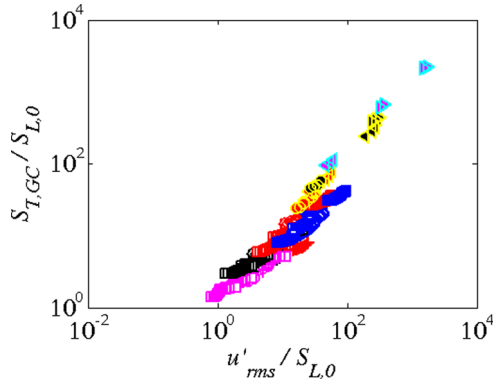

Fig. 8 Log-log plot of $S_{T,GC}$ as function of u'_{rms} normalized by $S_{L,0}$ at various mean flow velocities, H_2/CO ratios, and pressures for the 20 mm diameter burner (see Tables 1 and 2 for the legend)

Analysis of Flame Speed Data

***$S_{L,max}$* Normalization.** In this section, the data presented in Figs. 5 and 7 are correlated using the scaling law given by Eq. (2). The key input to this model is $S_{L,max}$, which is extracted from stretch sensitivity calculations, examples of which are given in Figs. 1 and 2.

Figure 9 plots the 12 mm diameter burner normalized by $S_{L,max}$. Note that the 10 atm, 5 atm, and 1 atm data sets collapse quite well individually but that there are systematic differences between them.

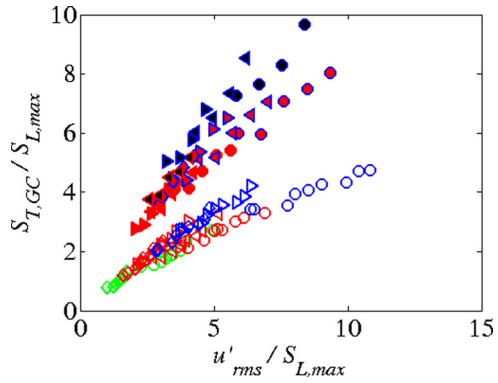

Fig. 9 $S_{T,GC}$ as a function of u'_{rms} normalized by $S_{L,max}$ at various mean flow velocities, H_2/CO ratios, and pressures using the 12 mm diameter burner (see Table 1 for the legend)

Figure 10 plots the result of normalizing all the 20 mm diameter burner data acquired at 1 atm by $S_{L,max}$. This data had the interesting behavior that all the data collapsed except for the 30 m/s CH_4/air case. Figure 10 has also been reproduced here, because it is difficult to see this collapse in Fig. 11, which plots the entire $S_{L,max}$ normalized 20 mm diameter burner data set.

From Fig. 11, we can make similar observations regarding the data of a given pressure collapsing reasonably well but not collapsing across pressures. However, this trend is not as clear-cut as in Fig. 9, because of the broad range in $S_{L,0}$ and $S_{L,max}$ present in this data set.

To summarize, the scaling law given by Eq. (2) successfully collapses the $S_{T,GC}$ across H_2/CO ratios and equivalence ratios for a given pressure. However, the scaling is unable to collapse the 30 m/s CH_4/air data or the data taken at different pressures.

Time Scale Correlations. As discussed in the introduction, chemical non-quasi-steady effects are one potential mechanism leading to the pressure sensitivity of $S_{T,GC}/S_{L,max}$. If the unsteady stretching of the flame leading points happens faster than the flame can respond, the local burning velocity at the leading point will be lower than its quasi-steady $S_{L,max}$ value. These effects can be incorporated into Eq. (2) by replacing $S_{L,max}$ with $\langle S_{L,max}(\omega)\rangle$, which is the ensemble-averaged frequency-dependent $S_{L,max}$. The resulting expression can then be divided by the steady-state $S_{L,max}$ to give

$$\frac{S_T}{S_{L,max}} = \frac{\langle S_{L,max}(\omega)\rangle}{S_{L,max}} + \frac{\langle u'_{rms}\rangle_{LP}}{S_{L,max}} \tag{5}$$

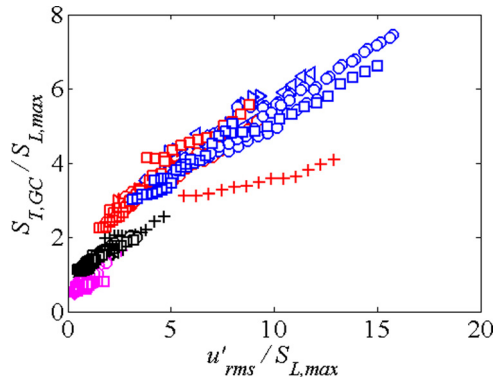

Fig. 10 $S_{T,GC}$ as function of u'_{rms} normalized by $S_{L,max}$ for all the data obtained using the 20 mm diameter burner at 1 atm (see Tables 1 and 2 for the legend)

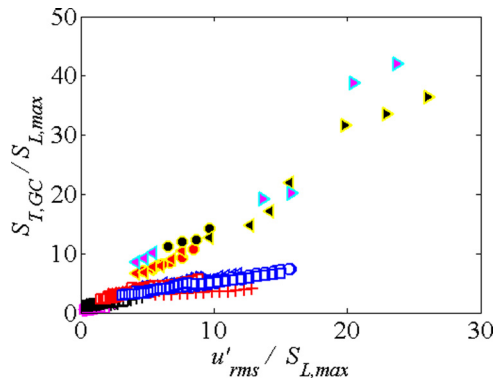

Fig. 11 $S_{T,GC}$ as function of u'_{rms} normalized by $S_{L,max}$ for all the data obtained using the 20 mm diameter burner at 1 atm (see Table 2 for the legend)

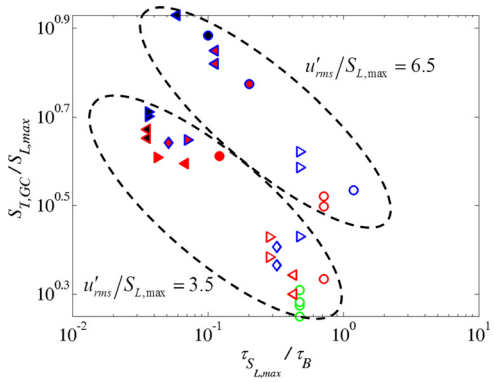

Fig. 12 Dependence of $S_{T,GC}/S_{L,max}$ upon $\tau_{S_{L,max}}/\tau_{flow}$ at fixed turbulence intensities, $u'_{rms}/S_{L,max} = 3.5$ and 6.5 for the 12 mm diameter burner where τ_{flow} is scaled as $D/U_0 = \tau_B$

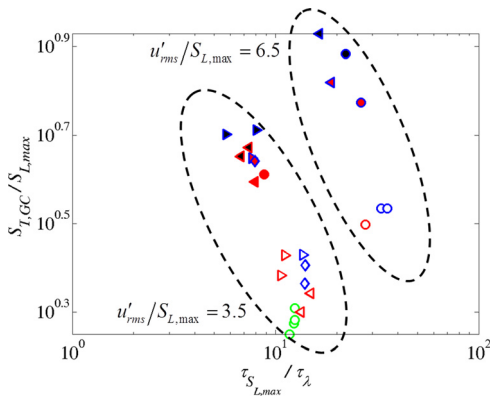

Fig. 13 Dependence of $S_{T,GC}/S_{L,max}$ upon $\tau_{S_{L,max}}/\tau_{flow}$ at fixed turbulence intensities, $u'_{rms}/S_{L,max} = 3.5$ and 6.5 for the 12 mm diameter burner where τ_{flow} is scaled as $l_\lambda/u'_{rms} = \tau_\lambda$

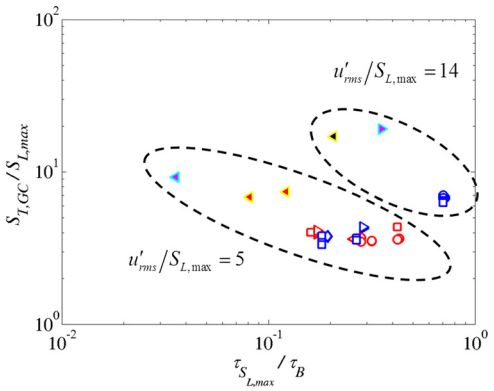

Fig. 14 Dependence of $S_{T,GC}/S_{L,max}$ upon $\tau_{S_{L,max}}/\tau_{flow}$ at fixed turbulence intensities, $u'_{rms}/S_{L,max} = 5$ and 14 for the 20 mm diameter burner where τ_{flow} is scaled as $D/U_0 = \tau_B$

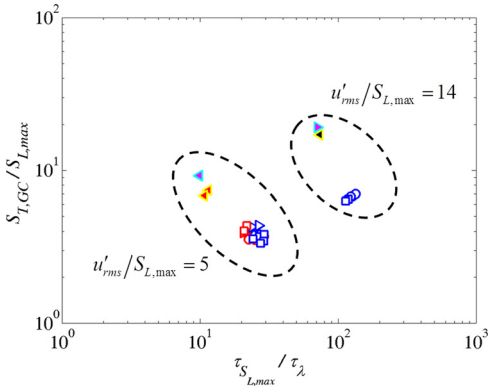

Fig. 15 Dependence of $S_{T,GC}/S_{L,max}$ upon $\tau_{S_{L,max}}/\tau_{flow}$ at fixed turbulence intensities, $u'_{rms}/S_{L,max} = 5$ and 14 for the 20 mm diameter burner where τ_{flow} is scaled as $l_\lambda/u'_{rms} = \tau_\lambda$

The degree of non-quasi-steadiness can be determined using a time scale ratio defined as $\tau_{S_{L,max}}/\tau_{flow}$, where $\tau_{S_{L,max}}$ is a chemical time scale associated with the highly stretched flamelets and τ_{flow} is a characteristic fluid mechanic time scale. The chemical time scale, $\tau_{S_{L,max}}$, is given by $\tau_{S_{L,max}} = \delta_F|_{S_{L,max}}/S_{L,max}$, where $\delta_F|_{S_{L,max}}$ is the flame thickness at $S_{L,max}$ calculated using $\delta_F = (T_b - T_u)/(dT/dx)_{max}$. We would then expect that $\langle S_{L,max}(\omega)\rangle/S_{L,max} \to 1$ as $\tau_{S_{L,max}}/\tau_{flow} \to 0$. In our previous works, we showed that, for constant $u'_{rms}/S_{L,max}$, the normalized turbulent flame speed correlated well with the normalized leading point time scale, as expected from Eq. (5), suggesting that a two-parameter scaling given by Eq. (6) may be a promising approach to model the turbulent flame speed [6].

$$\frac{S_T}{S_{L,max}} = f\left(\frac{\langle u'_{rms}\rangle_{LP}}{S_{L,max}}, \frac{\tau_{S_{L,max}}}{\tau_{flow}}\right) \tag{6}$$

This analysis is applied to the new data reported in this paper. Figure 12 plots $S_{T,GC}/S_{L,max}$ as a function of $\tau_{S_{L,max}}/\tau_{flow}$ at two representative fixed turbulence intensity conditions, $u'_{rms}/S_{L,max}$ of 3.5 and 6.5 for the 12 mm diameter burner. In Fig. 12, τ_{flow} is defined as a bulk flow time scale $\tau_B = D/U_0$ and as a Taylor time scale $\tau_\lambda = l_\lambda/u'_{rms}$ in Fig. 13. The Taylor scale, l_λ, is scaled as [42]

$$l_\lambda = l_{int}\sqrt{10}\,\mathrm{Re}_t^{-1/2} \tag{7}$$

where Re_t is defined as

$$\mathrm{Re}_t = \frac{u'_{rms} l_{int}}{\nu} \tag{8}$$

Note, from Fig. 12, the clear correlation between the normalized turbulent flame speed and time scale ratio across the entire range of pressure and fuel compositions. Slower chemistry is associated with lower values of the normalized turbulent flame speed, as would be expected, since the effective $S_{L,max}$ value of the non-quasi-steady flame is lower than its quasi-steady value.

Figure 13 plots these same data using the Taylor flow time scale. In contrast to the bulk flow time used in Fig. 12, τ_λ does have a pressure sensitivity through the Reynolds number. Note, from Fig. 13, that the range of normalized chemical time scales has decreased compared to in Fig. 12. This can be attributed to the fact that, although the chemical time scale decreases with pressure as $\tau_{S_{L,max}} \sim p^{-1}$ [6], the Taylor time scale decreases with pressure as $\tau_\lambda \sim p^{-1/2}$. Also note that $\tau_{S_{L,max}}/\tau_{flow}$ is greater than 1, suggesting that the leading point is non-quasi-steady with respect to the Taylor time scale.

Similar analyses were performed for the 20 mm data, and the results are shown in Figs. 14 and 15. The same trends seen in Fig. 12 are also seen here, namely the correlation between the turbulent flame speed and the time scale ratio across the range of mixtures and conditions. Also as before, the range in the normalized time scale is decreased when the Taylor time scale is utilized, and the leading point appears non-quasi-steady with respect to the Taylor time scale.

Concluding Remarks

This paper has shown that a broad range of fuel composition and pressure data can be correlated with the maximum laminar flame speed, $S_{L,max}$, and a chemical time scale ratio scaling. In particular, it was suggested that pressure effects influence the

turbulent burning velocity by altering how well the flame's internal chemistry can track the time-varying stretch rate at the leading point. If this assertion is true, then it clearly indicates the strong coupling effects of stretch and pressure. In particular, a key feature of this argument is that, in flames where $S_{L,\max}/S_{L,0} \gg 1$, non-quasi-steady effects can significantly alter the burning velocity of the leading point. This argument also suggests then that non-quasi-steady effects should have much less effect on mixtures with weak stretch sensitivity, where $S_{L,\max}/S_{L,0} \sim 1$.

Returning to the data, it must also be emphasized that the data, when normalized by $S_{L,\max}$, showed a clear correlation with pressure. Thus, any parameter that also correlates with pressure will also do a reasonable job of scaling the pressure effects. In particular, the Reynolds number linearly increases with pressure. Thus, these pressure effects could also be correlated with Reynolds number, an approach used in the correlation from Bradley et al. [12,13]. In addition, the Taylor and Kolmogorov length scales also have a Reynolds number and, therefore, a pressure sensitivity as shown in Eq. (9)

$$\frac{l_{\text{int}}}{\eta} \sim \text{Re}_t^{-3/4} \tag{9}$$

where η is the Kolmogorov length scale. Thus, these pressure effects could also be scaled using a length-scale ratio.

These results indicate that additional data is needed to differentiate between time scale, length scale, and other Reynolds number effects. We are currently exploring a broadened set of experimental conditions that will enable differentiation between time scale, length scale, and Reynolds number effects on the turbulent burning velocity.

Acknowledgment

This research was partially supported by the University Turbine Systems Research program, Mark Freeman, contract monitor, under contract DE-FC21-92MC29061, and by University of California, Irvine through a subcontract with the California Energy Commission. The authors are grateful to Mr. Bobby Noble, Brad Ochs, and Dave Shaw for their invaluable assistance in designing and installing the high-pressure test facility. The authors also gratefully acknowledge Mr. Ramon Romero for his assistance in assembling the experimental facility and data collection.

Nomenclature

$\overline{A}_{\langle c \rangle}$ = mean flame area associated with given $\langle c \rangle$ contour
$\langle c \rangle$ = average progress variable contour
D = burner diameter
Ka_η = Karlovitz number based on the Kolmogorov time scale
l_{int} = turbulent integral length scale
l_M = Markstein length
l_λ = turbulent Taylor length scale
$\dot{m}_R$ = reactant mass flow rate
p = pressure
Re_t = turbulent Reynolds number
S_L = stretched laminar flame speed
$S_{L,\max}$ = maximum stretched laminar flame speed
$S_{L,0}$ = unstretched laminar flame speed
S_T = turbulent flame speed
$S_{T,\text{GC}}$ = global turbulent consumption speed
T = temperature
u'_{rms} = root mean square turbulence fluctuations
U_0 = mean axial velocity
x = distance along flame normal
δ_F = flame thickness
κ = stretch rate
κ_{ext} = extinction stretch rate
ρ_R = reactant density
τ_B = fluid mechanical time scale given by D/U_0
τ_{flow} = characteristic fluid mechanical time scale
$\tau_{S_{L,\max}}$ = chemical time scale defined as $\delta_F|_{S_{L,\max}}/S_{L,\max}$
τ_λ = Taylor time scale given by $l_\lambda/u'_{\text{rms}}$
ϕ = equivalence ratio

Appendix

The consumption speed measurements obtained using the 20 mm diameter burner at 1 atm and 300 K are reproduced in Figs. 16–18 in order to facilitate the discussion on the modeling of these data. The parameter ranges explored in this study along with the symbol type and color scheme are summarized in Table 2.

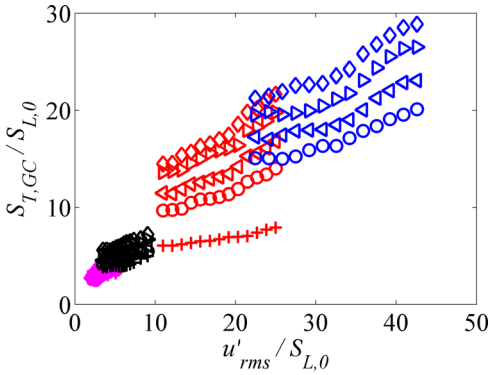

Fig. 16 $S_{T,\text{GC}}$ as function of u'_{rms} normalized by $S_{L,0}$ for the constant $S_{L,0}$ studies using the 20 mm diameter burner (see Table 1 for the legend)

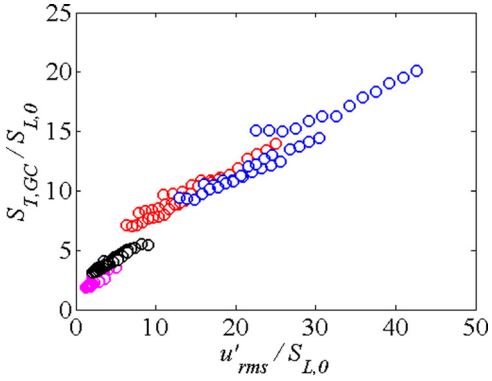

Fig. 17 $S_{T,\text{GC}}$ as function of u'_{rms} normalized by $S_{L,0}$ for the varying $S_{L,0}$ studies for H_2 = 30% mixture using the 20 mm diameter burner (see Table 2 for legend)

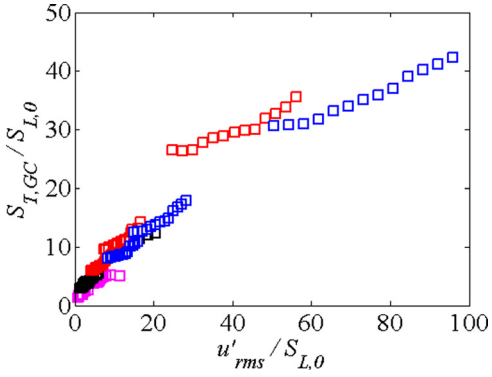

Fig. 18 $S_{T,\text{GC}}$ as function of u'_{rms} normalized by $S_{L,0}$ for the varying $S_{L,0}$ studies for H_2 = 60% mixture using the 20 mm diameter burner (see Table 2 for legend)

Figure 16 plots the consumption speed data for the constant $S_{L,0}$ studies, while Figs. 17 and 18 plot the data for the varying $S_{L,0}$ for the 30% and 60% H_2 content mixtures, respectively.

References

[1] Lieuwen, T., McDonell, V., Petersen, E., and Santavicca, D., 2008, "Fuel Flexibility Influences on Premixed Combustor Blowout, Flashback, Autoignition, and Stability," ASME J. Eng. Gas Turbines Power, **130**, p. 011506.

[2] Lipatnikov, A. N., and Chomiak, J., 2002, "Turbulent Flame Speed and Thickness: Phenomenology, Evaluation, and Application in Multi-Dimensional Simulations," Prog. Energy Combust. Sci., **28**, pp. 1–74.

[3] Poinsot, T., and Veynante, D., 2005, *Theoretical and Numerical Combustion*, RT Edwards, Philadelphia.

[4] Driscoll, J. F., 2008, "Turbulent Premixed Combustion: Flamelet Structure and Its Effect on Turbulent Burning Velocities," Prog. Energy Combust. Sci., **34**, pp. 91–134.

[5] Venkateswaran, P., Marshall, A., Shin, D. H., Noble, D., Seitzman, J., and Lieuwen, T., 2011, "Measurements and Analysis of Turbulent Consumption Speeds of H_2/CO Mixtures," Combust. Flame, **158**, pp. 1602–1614.

[6] Venkateswaran, P., Marshall, A., Seitzman, J., and Lieuwen, T., 2013, "Pressure and Fuel Effects on Turbulent Consumption Speeds of H_2/CO Blends," Proc. Combust. Inst., **34**, pp. 1527–1535.

[7] Richards, G. A., and Casleton, K. H., 2009, "Gasification Technology to Produce Synthesis Gas," *Synthesis Gas Combustion: Fundamentals and Applications*, T. C. Lieuwen, V. Yang, and R. A. Yetter, eds., CRC, Boca Raton, FL, p. 403.

[8] Lefebvre, A. H., 1998, *Gas Turbine Combustion*, CRC, Boca Raton, FL.

[9] Lipatnikov, A. N., and Chomiak, J., 2005, "Molecular Transport Effects on Turbulent Flame Propagation and Structure," Prog. Energy Combust. Sci., **31**, pp. 1–73.

[10] Kido, H., Nakahara, M., Hashimoto, J., and Barat, D., 2002, "Turbulent Burning Velocities of Two-Component Fuel Mixtures of Methane, Propane and Hydrogen," JSME Int. J., Ser. B, **45**, pp. 355–362.

[11] Law, C. K., 2006, *Combustion Physics*, Cambridge University Press, New York.

[12] Bradley, D., Lawes, M., and Mansour, M. S., 2011, "Correlation of Turbulent Burning Velocities of Ethanol-Air, Measured in a Fan-Stirred Bomb Up to 1.2 MPa," Combust. Flame, **158**, pp. 123–138.

[13] Bradley, D., Lawes, M., Liu, K., and Mansour, M. S., 2013, "Measurements and Correlations of Turbulent Burning Velocities Over Wide Ranges of Fuels and Elevated Pressures," Proc. Combust. Inst., **34**, pp. 1519–1526.

[14] Wu, M. S., Kwon, S., Driscoll, J. F., and Faeth, G. M., 1990, "Turbulent Premixed Hydrogen/Air Flames at High Reynolds Numbers," Combust. Sci. Technol., **73**, pp. 327–350.

[15] Daniele, S., Jansohn, P., Mantzaras, J., and Boulouchos, K., 2011, "Turbulent Flame Speed for Syngas at Gas Turbine Relevant Conditions," Proc. Combust. Inst., **33**, pp. 2937–2944.

[16] Kobayashi, H., Tamura, T., Maruta, K., Niioka, T., and Williams, F. A., 1996, "Burning Velocity of Turbulent Premixed Flames in a High-Pressure Environment," Proc. Combust. Inst., **26**, pp. 389–396.

[17] Lipatnikov, A. N., and Chomiak, J., 1998, "Lewis Number Effects in Premixed Turbulent Combustion and Highly Perturbed Laminar Flames," Combust. Sci. Technol., **137**, pp. 277–298.

[18] Karpov, V. P., Lipatnikov, A. N., and Zimont, V. L., 1997, "Flame Curvature as a Determinant of Preferential Diffusion Effects in Premixed Turbulent Combustion," *Advances in Combustion Science: In Honor of Ya. B. Zel'dovich*, Vol. 173, W. A. Sirignano, A. G. Merzhanov, and L. De Luca, eds., AIAA, Reston, VA, pp. 235–250.

[19] Kuznetsov, V. R., and Sabel'nikov, V. A., 1986, "Turbulent Combustion of a Homogenous Mixture," *Turbulence and Combustion*, V. R. Kuznetsov and V. A. Sabel'nikov, eds., Hemisphere, Moscow, p. 362.

[20] Dinkelacker, F., Manickam, B., and Muppala, S. P. R., 2011, "Modelling and Simulation of Lean Premixed Turbulent Methane/Hydrogen/Air Flames With an Effective Lewis Number Approach," Combust. Flame, **158**, pp. 1742–1749.

[21] Duclos, J. M., Veynante, D., and Poinsot, T., 1993, "A Comparison of Flamelet Models for Premixed Turbulent Combustion," Combust. Flame, **95**, pp. 101–117.

[22] Damköhler, G., 1940, "Der Einfluss der Turbulenz auf die Flammengeschwindigkeit in Gasgemischen," Z. Elektrochem. **46**, 601–652 (English translation NASA Tech. Mem. 1112, 1947).

[23] Egolfopoulos, F. N., 1994, "Geometric and Radiation Effects on Steady and Unsteady Strained Laminar Flames," Proc. Combust. Inst., **25**, pp. 1375–1381.

[24] Amato, A., Day, M. S., Cheng, R. K., Bell, J., and Lieuwen, T., 2012, "Leading Point Statistics of a Turbulent, Lean, H_2-Air Flame," Central States Section Spring Technical Meeting, Dayton, OH.

[25] Peiyong, W., Hu, S., Wehrmeyer, J. A., and Pitz, R. W., 2004, "Stretch and Curvature Effects on Flames," 42nd AIAA Aerospace Sciences Meeting and Exhibit, Rena, NV, January 5–8, AIAA Paper No. 2004-148.

[26] Im, H. G., and Chen, J. H., 2000, "Effects of Flow Transients on the Burning Velocity of Laminar Hydrogen/Air Premixed Flames," Proc. Combust. Inst., **28**, pp. 1833–1840.

[27] Kitagawa, T., Nakahara, T., Maruyama, K., Kado, K., Hayakawa, A., and Kobayashi, S., 2008, "Turbulent Burning Velocity of Hydrogen-Air Premixed Propagating Flames at Elevated Pressures," Int. J. Hydrogen Energy, **33**, pp. 5842–5849.

[28] Liu, C.-C., Shy, S. S., Peng, M.-W., Chiu, C.-W., and Dong, Y.-C., 2012, "High-Pressure Burning Velocities Measurements for Centrally-Ignited Premixed Methane/Air Flames Interacting With Intense Near-Isotropic Turbulence at Constant Reynolds Numbers," Combust. Flame, **159**, pp. 2608–2619.

[29] Chiu, C.-W., Dong, Y.-C., and Shy, S. S., 2012, "High-Pressure Hydrogen/Carbon Monoxide Syngas Turbulent Burning Velocities Measured at Constant Turbulent Reynolds Numbers," Int. J. Hydrogen Energy, **37**, pp. 10935–10946.

[30] Gouldin, F., and Cheng, R. K., 2010, International Workshop on Premixed Turbulent Flames, http://energy.lbl.gov/aet/combustion/workshop/workshop.html

[31] Cheng, R. K., 2009, "Turbulent Combustion Properties of Premixed Syngas," *Synthesis Gas Combustion: Fundamentals and Applications*, T. C. Lieuwen, V. Yang, and R. A. Yetter, eds., CRC, Boca Raton, FL, p. 403.

[32] Marshall, A., Venkateswaran, P., Noble, D., Seitzman, J., and Lieuwen, T., 2011, "Development and Characterization of a Variable Turbulence Generation System," Exp. Fluids, **51**, pp. 611–620.

[33] Dasch, C., 1992, "One-Dimensional Tomography—A Comparison of Abel, Onion-Peeling, and Filtered Backprojection Methods," Appl. Opt., **31**, pp. 1146–1152.

[34] Ballal, D., and Lefebvre, A., 1975, "The Structure and Propagation of Turbulent Flames," Proc. R. Soc. London, Ser. A, **344**, pp. 217–234.

[35] Smallwood, G., and Gülder, Ö., 1995, "Characterization of Flame Front Surfaces in Turbulent Premixed Methane/Air Combustion," Combust. Flame, **101**, pp. 461–470.

[36] Kee, R. J., Grcar, J. F., Smooke, M., and Miller, J., 1983, "PREMIX: A Fortran Program for Modeling Steady Laminar One-Dimensional Premixed Flames," Sandia National Laboratories, Livermore, CA, Report No. SAND85-8240.

[37] Davis, S. G., Joshi, A. V., Wang, H., and Egolfopoulos, F., 2005, "An Optimized Kinetic Model of H_2/CO Combustion," Proc. Combust. Inst., **30**, pp. 1283–1292.

[38] Borghi, R., 1985, "On the Structure and Morphology of Turbulent Premixed Flames," *Recent Advances in the Aerospace Sciences (A 85-47304 23-31)*, Plenum, New York, pp. 117–138.

[39] Peters, N., 1999, "The Turbulent Burning Velocity for Large-Scale and Small-Scale Turbulence," J. Fluid Mech., **384**, pp. 107–132.

[40] Kee, R. J., Miller, J. A., Evans, G. H., and Dixon-Lewis, G., 1989, "A Computational Model of the Structure and Extinction of Strained, Opposed Flow, Premixed Methane-Air Flames," Proc. Combust. Inst., **22**, pp. 1479–1494.

[41] Wu, C. K., and Law, C. K., 1985, "On the Determination of Laminar Flame Speeds From Stretched Flames," Proc. Combust. Inst., **20**, pp. 1941–1949.

[42] Pope, S., 2000, *Turbulent Flows*, Cambridge University Press, New York.